



# Estimating Hidden Cholera Burden and Intervention Effectiveness

Murshed Ahmed Ovi<sup>1</sup> · Andrei Afilipoaei<sup>1</sup> · Hao Wang<sup>1</sup> 

Received: 17 October 2024 / Accepted: 1 May 2025

© The Author(s), under exclusive licence to the Society for Mathematical Biology 2025

## Abstract

Cholera remains a significant public health threat in many parts of the world, with differing levels of compliance to intervention strategies and undocumented cases contributing to reservoir contamination with *Vibrio cholerae* at varying rates alongside reported cases. To address this, we incorporate an inapparent cholera-infected compartment into the iSIR model and equip it with parameters depicting vaccination and compliance levels for water and food sanitation, handwashing, and safe fecal disposal. Our model shows that the bacteria shedding from the inapparent infection can significantly affect the spread of cholera. Also, we identify that lowering the bacteria ingestion rate among the susceptible and controlling the bacteria shedding from reported infected are two key components for obtaining a disease-free state in the long run. The model fitting to cholera outbreaks in Haiti, Kenya, Malawi, and Zimbabwe implies that at least 88.5% of cases are inapparent, with the first reporting appearing up to 11 weeks after the start of the outbreak. Additionally, we find that the combination of water and food sanitation and handwashing is the most effective intervention strategy for reducing the cholera outbreak peak if compliance with these measures remains at moderate or high levels. However, with low compliance, safe fecal disposal of the reported infected individuals combined with vaccination coverage of the susceptible population is suggested to obtain the lowest outbreak peak.

**Keywords** Hidden Cholera Burden · Interventions

## 1 Introduction

Cholera, an intestinal sickness caused by the *Vibrio cholerae* bacteria, primarily arises from polluted water and food sources (Centers for Disease Control and Prevention 2024b; Nelson et al. 2009). The contagion can rapidly spread in communities where access to safe drinking water, proper sanitation, and adequate hygiene are lacking,

---

✉ Hao Wang  
hao8@ualberta.ca

<sup>1</sup> Mathematical and Statistical Sciences, University of Alberta, Edmonton, AB T6G 2G1, Canada

especially in areas with limited medical resources (Taylor et al. 2015). The risk of illness after exposure to a bacteria-contaminated reservoir depends on the pathogen density within the reservoir and the individual's immune response. Although the precise threshold of bacterial infection remains uncertain, it is generally estimated at least  $10^3$  to  $10^6$  *Vibrio cholerae* bacteria must be ingested to cause an infection (Colwell et al. 1996; Joh et al. 2009; Levine et al. 1981). Once a sufficiently large quantity of bacteria enters the human body, *V. cholerae* passes through the mucus layer of the gut and begins to spread in the epithelium (Mandal et al. 2011). The bacteria then produce a cholera toxin (CT), which causes the infected individual to discharge disproportionately high levels of fluids and electrolytes in the form of diarrhea (Mandal et al. 2011). As the illness progresses, the significant fluid loss experienced by the infected individual can cause severe dehydration, kidney failure, and, in extreme cases, death (Centers for Disease Control and Prevention 2024b; Mandal et al. 2011). Fortunately, even in severe cases of the disease, a rapid treatment response can reduce mortality to as little as 1% (Mandal et al. 2011), and individuals who survive a cholera infection enjoy a strong and long-term immunity to the illness for a period of at least 3 years (Harris 2018).

*Vibrio cholerae* is primarily a human pathogen (Harris 2018), though it also persists in aquatic environments as a part of its natural life-cycle (Conner et al. 2016). The infection has an incubation period of approximately 18 hours to 5 days, but progresses rapidly thereafter, with severe cases bringing about the death of the patient in as little as 6-12 hours after the onset of symptoms (Mandal et al. 2011). Luckily, cholera is usually not so severe, with approximately 90% of cases being moderate or even mild and thereby being indistinguishable from other instances of aggravated diarrhea (Centers for Disease Control and Prevention 2024b; Mandal et al. 2011). Additionally, estimates suggest that 60-90% of cholera cases are asymptomatic, as reported by Fung (2014) (Fung 2014), with Chao et al. estimating this figure at around 80% (Chao et al. 2011). Moreover, King et al. (2008) also noted a wide range of estimates for asymptomatic cases, from 75% to 99%, and provided evidence supporting a high proportion of asymptomatic cholera cases (King et al. 2008). Furthermore, Fung (2014) points out that only symptomatic cases are usually detected in surveillance data (Fung 2014), although evidence suggests that even symptomatic cholera cases are subject to underreporting (Ali et al. 2015; Bertuzzo et al. 2011; Hegde et al. 2024; Mwaba et al. 2020). Consequently, Fung (2014) emphasizes the importance of considering these underreported and asymptomatic cases in modeling efforts to capture cholera transmission dynamics accurately (Fung 2014). Few modeling efforts have considered these explicitly (Lee et al. 2020; Kirpich et al. 2015). Meanwhile, both asymptomatic and symptomatic individuals shed *Vibrio cholerae* at varying rates, thereby fueling the spread of the disease. For instance, previous models have taken asymptomatic cases to have only one-tenth or one-hundredth of the bacterial shedding of symptomatic cases (Chao et al. 2011; Miller Neilan et al. 2004).

While treating infected individuals using oral rehydration solutions (ORS) or intravenous fluids is relatively straightforward, the hurdle arises from the limitations of healthcare systems in many developing countries. These systems often fall short of providing essential health services, including adequate treatment, access to a clean

water supply, and proper hygiene facilities, especially in the face of a sudden and rapid surge of cholera outbreaks (Longini et al. 2007; Mukandavire et al. 2011; Zuckerman et al. 2007). Although the first cholera pandemic emerged out of the Ganges Delta in India in 1817, in recent times, the majority of cholera cases, about 60%, persist in the sub-Saharan African region each year (Ali et al. 2015; Mwaba et al. 2020). The cholera epidemic in South Africa from 2000–2001 resulted in the tragic loss of 265 lives and a total of 117,147 infections (Hemson et al. 2006). Recent severe outbreaks in several developing countries have underscored the persistence of cholera around the world, including Yemen in 2016–2018 (over 1 million suspected cases), Haiti in 2010–2012 (545,000 reported cases), Zimbabwe in 2008–2009 (almost 100,000 reported cases), and Zambia in 2017–2018 (5905 suspected cases) (Sinyange et al. 2018; Tappero and Tauxe 2011; Yang and Wang 2019).

Given its historical prevalence, cholera continues to exert a significant global toll, marked by seven recorded pandemics throughout human history (Deen 2020). The ongoing high burden of cholera is primarily attributed to the widespread absence of basic safe drinking water and sanitation in numerous regions worldwide (Deen 2020; World Health Organization 2023). A staggering estimate in 2017 indicates that over 2 billion people globally consume water from potentially fecally contaminated sources and 2.3 billion lack essential sanitation facilities, exposing them to cholera and other waterborne infections (Global Task Force on Cholera Control (GTFCC) 2017). In October 2017, the Global Task Force on Cholera Control (GTFCC) initiated a comprehensive global strategy aimed at a 90% reduction in cholera-related deaths and the complete elimination of cholera in 20 out of the 47 countries currently grappling with the disease by the year 2030 (Global Task Force on Cholera Control (GTFCC) 2017). Enhancing Water, Sanitation, and Hygiene (WASH) infrastructure is the primary non-pharmaceutical strategy for effective cholera control (Taylor et al. 2015). However, public compliance with these prevention measures can be the deciding factor for success. For example, despite increased awareness efforts, cholera remains a public health problem in Kenya; while 63.8% of respondents recognized the importance of treating drinking water, only 51.3% practiced water treatment (Orimbo et al. 2020). A study in Lebanon revealed that approximately 71.43% of respondents were careless with regards to cholera, despite possessing good knowledge and knowing the correct practices (Akel et al. 2023). Therefore, identifying high-priority interventions and determining the necessary level of public compliance to achieve a disease-curtailed outcome is crucial.

Dating back to the 18th century with Bernoulli (Bernoulli 1766), mathematical modeling for infectious diseases has become indispensable in epidemiological research (Daley and Gani 1999). These models serve as powerful tools for understanding infection, predicting epidemic progression, comparing interventions, and offering guidelines for outbreak management (Hethcote 2000). Substantial progress has already been made in modelling the complex transmission of cholera. In this study, we extend the *iSIR* model, originally developed by Joh et al. in 2009 (Joh et al. 2009) to account for indirect transmission and notable for including the minimum infectious dose required for infection, by adding an inapparent infected compartment ( $I^u$ ) to create an *iSI<sup>u</sup>I<sup>r</sup>R* model. This new compartment  $I^u$  accounts for both unreported

asymptomatic and underreported symptomatic cholera cases and  $I^r$  represents the reported infected population. Our model also incorporates people's compliance with various preventive measures, including safe food and drinking water, handwashing, safe fecal disposal, and vaccination. Our objectives are to explore how the inapparent compartment affects disease spread, to detect the percentage of reported cases, to assess how different levels of public adherence to the prevention measures influence disease dynamics, and to identify the most effective pairs of non-pharmaceutical interventions for minimizing disease spread. To address these objectives, we perform both qualitative and quantitative analyses of the model and its interventions. Also, the model is validated by fitting it to cholera surveillance data from multiple countries (Africa Centres for Disease Control and Prevention 2024; Pan American Health Organization 2024; Rinaldo et al. 2012).

## 2 Model Formulation and Analyses

To accurately capture the dynamics of cholera, it is essential to incorporate the consumption of contaminated water and food from sources (reservoirs) such as rivers, dams, wells, ponds, etc. as a primary driver of indirect transmission (Centers for Disease Control and Prevention 2024a, b; Nelson et al. 2009). The presence of an immunological threshold (Joh et al. 2009) makes it reasonable to consider a minimum infectious dose (MID) of *Vibrio cholerae* to be infected (Murphy et al. 2007). Additionally, the model should account for the proportion of unreported asymptomatic and under-reported symptomatic cases, as highlighted in the introduction, alongside the reported symptomatic cases. Given these considerations, we propose an extension of the iSIR model (Joh et al. 2009) to the  $iSI^uI^rR$  ( $S$  as Susceptible class,  $I^u$  as Inapparent class including both unreported asymptomatic and under-reported symptomatic infected cases,  $I^r$  as Reported Symptomatic Infected class,  $R$  as Recovered class, and  $B$  as *Vibrio Cholerae* density in the reservoir) model. This extension is expected to give an advantage in reducing the possibility of cholera outbreak overestimation by measuring the ratio between reported cholera cases and unobserved infections, highlighting the role of these unmeasured infections in the spread of cholera. It also includes people's compliance levels with different intervention strategies to reduce cholera's spread. We take  $c_s$  and  $c_h$  to denote the proportion of compliance with water and food sanitation and handwashing among susceptible individuals respectively. In addition,  $c_{f_u}$  refers to the proportion of compliance with safe fecal disposal by inapparent infected individuals, while  $c_{f_r}$  applies to reported symptomatic infected individuals. The intended interactions among the compartments are illustrated in the schematic diagram (Fig. 1) and framed through the set of differential equations in (1).

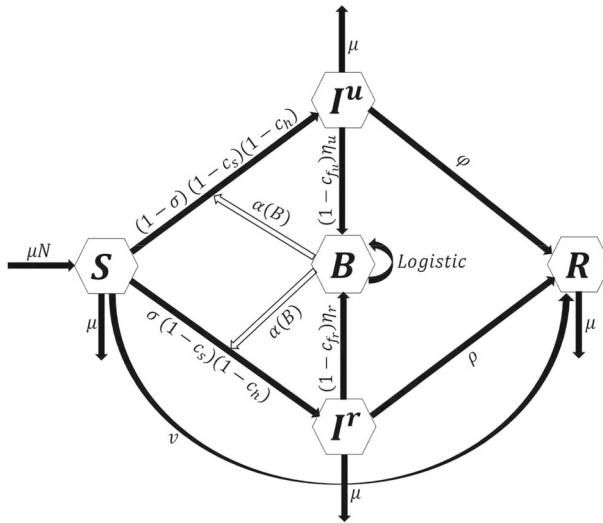


**Fig. 1** Schematic diagram of compliance incorporated  $iSI^u I^r R$  model with pathogen density, where the white arrow represents indirect transmission

$$\begin{aligned}
 \frac{dS}{dt} &= \mu N - (1 - c_s)(1 - c_h)\alpha(B)S - vS - \mu S, \\
 \frac{dI^u}{dt} &= (1 - \sigma)(1 - c_s)(1 - c_h)\alpha(B)S - \phi I^u - \mu I^u, \\
 \frac{dI^r}{dt} &= \sigma(1 - c_s)(1 - c_h)\alpha(B)S - \rho I^r - \mu I^r, \\
 \frac{dR}{dt} &= vS + \phi I^u + \rho I^r - \mu R, \\
 \frac{dB}{dt} &= r_1 B \left(1 - \frac{B}{K}\right) + (1 - c_{f_u}) \eta_u I^u + (1 - c_{f_r}) \eta_r I^r.
 \end{aligned}
 \tag{1}$$

Here,  $\mu$  is the average birth and mortality rate based on national life expectancy;  $v$  represents the rate of vaccination among the susceptible population;  $\phi$  and  $\rho$  are the recovery rates for  $I^u$  and  $I^r$ ; and  $\eta_u$  and  $\eta_r$  are the respective shedding rates for  $I^u$  and  $I^r$ . The details of these variables and parameters and their units and ranges are displayed in Table 1 in the Appendix D. It is evident from the system that the total at-risk population  $N$  participating in the model dynamics is conserved, so  $R = N - S - I^u - I^r$ . Hence,  $S$ ,  $I^u$ ,  $I^r$ , and  $B$  are the targeted compartments for further analyses. Note that the already compliant people to the selected control measures neither get infected ( $c_s = c_h = 1$ ) nor contribute to bacterial transmission ( $c_{f_u} = c_{f_r} = 1$ ), so they don't participate in the disease dynamics considered in our model. Finally, the transmissibility  $\alpha(B)$  of Cholera in Eq. (1) is defined as an increasing function of *Vibrio cholerae* density  $B$  based on the concept of the minimum infectious dose

(MID), the threshold pathogen density required for infection ( $c$ ), as described by Joh et al. (2009) (Joh et al. 2009). Mathematically it appears as follows:

$$\alpha(B) = \begin{cases} 0 & \text{if } B < c, \\ \frac{\beta_e(B-c)}{(B-c)+H} & \text{if } B \geq c. \end{cases} \tag{2}$$

with  $H$  being half saturation bacteria density and  $\beta_e$  denotes the ingestion rate of *vibrio cholera* from the contaminated environment.

**Proposition 1** *The set  $\Gamma = \{S, I^u, I^r, R, B \geq 0 : S + I^u + I^r + R = N, \text{ and } B < B_{max}\}$  defines a forwardly invariant region of the system (1), where*

$$B_{max} = \frac{Kr_1 + K\sqrt{r_1^2 + 4(1-c_f)\frac{r_1\eta N}{K}}}{2r_1} \text{ with } c_f = \min\{c_{f_u}, c_{f_r}\} \text{ and } \eta = \max\{\eta_u, \eta_r\}.$$

Please see Appendix A for the proof.

Now, we will use the following quantities to create a non-dimensionalized version of the system (1) and conduct further analyses.

$$S_1 = \frac{S}{N}; I_1^u = \frac{I^u}{N}; I_1^r = \frac{I^r}{N}; B_1 = \frac{B}{K}; \tau = \mu t; \beta = \frac{\beta_e}{\mu}; c_1 = \frac{c}{K}; p_s = \frac{v+\mu}{\mu}; p_u = \frac{\phi+\mu}{\mu}; p_r = \frac{\rho+\mu}{\mu}; q_u = \frac{\eta_u N}{\mu K}; q_r = \frac{\eta_r N}{\mu K}; \tilde{r}_1 = \frac{r_1}{\mu}, \lambda = \frac{H}{K}.$$

Hence, the non-dimensionalized version is given in (3).

$$\begin{aligned} \frac{dS_1}{d\tau} &= 1 - (1 - c_s)(1 - c_h)\alpha_1(B)S_1 - p_s S_1, \\ \frac{dI_1^u}{d\tau} &= (1 - \sigma)(1 - c_s)(1 - c_h)\alpha_1(B)S_1 - p_u I_1^u, \\ \frac{dI_1^r}{d\tau} &= \sigma(1 - c_s)(1 - c_h)\alpha_1(B)S_1 - p_r I_1^r, \\ \frac{dB_1}{d\tau} &= \tilde{r}_1 B_1 (1 - B_1) + (1 - c_{f_u}) q_u I_1^u + (1 - c_{f_r}) q_r I_1^r, \end{aligned} \tag{3}$$

where

$$\alpha_1(B_1) = \begin{cases} 0 & \text{if } B_1 < c_1, \\ \frac{\beta(B_1-c_1)}{(B_1-c_1)+\lambda} & \text{if } B_1 \geq c_1. \end{cases}$$

This non-dimensionalized model 3 is used to conduct further analyses. Without any intervention measures i.e.  $c_s = 0; c_h = 0; v = 0; c_{f_u} = 0; c_{f_r} = 0$ , if the minimum infectious dose ( $c$ ) is less than the carrying capacity of *vibrio cholera* ( $K$ ) in a particular region, the disease persists in the long run, making it endemic. On the other hand, if the minimum infectious dose ( $c$ ) exceeds the carrying capacity, cholera may either vanish from the region or become endemic; however, a sufficiently small pathogen enhancement ratio ( $\zeta$  - a term introduced by Joh et al. (2009)) ensures that a disease-free environment is achieved eventually. Where the pathogen enhancement ratio is expressed as follows,

$$\zeta = \left[ \frac{(1 - \sigma)q_u}{\tilde{r}_1 p_u} + \frac{\sigma q_r}{\tilde{r}_1 p_r} \right] \times \frac{\beta}{\beta + 1}, \tag{4}$$

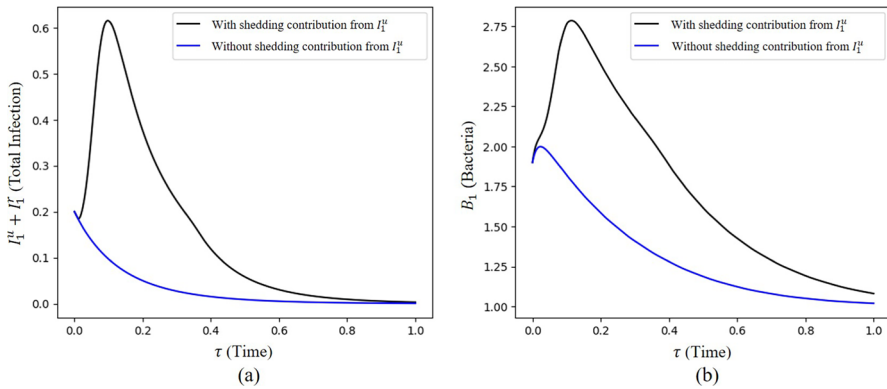


**Fig. 2** The contribution of inapparent infected  $I_1^u$  in spreading cholera. When the shedding contribution of  $I_1^u$  is added to the contribution of  $I_1^r$ , (a) shows a significant rise in the total infection and (b) highlights the surge of *Vibrio cholera* density responsible for this increased infection. Parameters value used are  $c_s = 0.0$ ,  $c_h = 0.0$ ,  $v = 0.0$ ,  $c_{fu} = 0.0$  (with)/1.0 (without),  $\beta = 100$ ,  $c_1 = 2$ ,  $p_s = 1$ ,  $p_u = 10$ ,  $p_r = 5$ ,  $q_u = 45$ ,  $q_r = 450$  (Color figure online)

in original terms, it looks like the following,

$$\zeta = \left[ \frac{(1 - \sigma)\eta_u}{\phi + \mu} + \frac{\sigma\eta_r}{\rho + \mu} \right] \times \frac{\mu N}{r_1 K} \times \frac{\beta_e}{\beta_e + \mu}. \tag{5}$$

Please see the Appendix B in support of these results.

### 2.1 Inapparent Infection Contribution and Global Sensitivity Analysis

As outlined in the Introduction, there is a significant difference between the shedding rate of asymptomatic and symptomatic patients. The inapparent infected group consists of both unreported asymptomatic individuals and symptomatic patients missing from cholera data. Consequently, the shedding rate corresponding to this group may vary across different outbreaks. Fig. 2 illustrates the substantial role inapparent infections can play in increasing *Vibrio cholerae* density in the reservoir. Although reported cases contribute to bacterial growth, this alone is insufficient to raise the density above the minimum infectious dose, as reflected in the blue curve where no significant rise in infections is observed. In contrast, the black curve demonstrates how declining infections escalated into a large outbreak, driven by a sharp increase in bacterial density attributed to the shedding from inapparent infected individuals. In this figure we have assumed that the inapparent infected shed ten times less than the reported infected people, following Miller Neilan et al. (2004). However, it is important to note that the shedding contribution from inapparent has to be large enough to create significant cholera spread (see Fig. 14 in Appendix B as an example). This difference in shedding rate between the two groups is estimated while fitting our model to different country’s data.

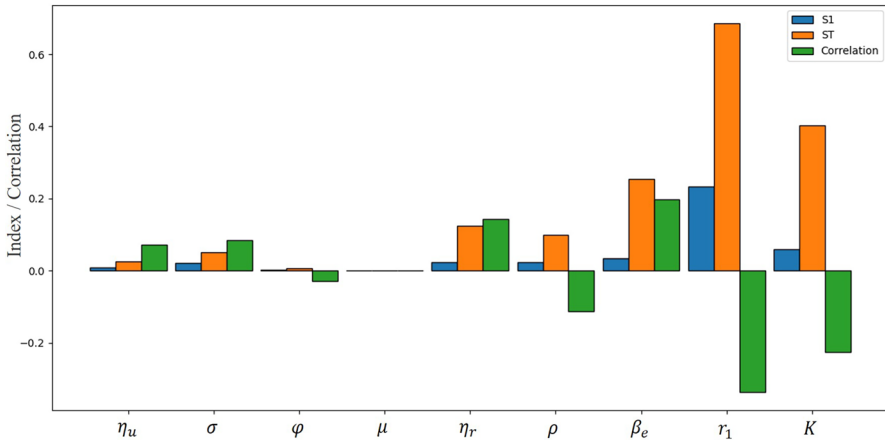


**Fig. 3** The global sensitivity analyses to identify key parameters driving the pathogen enhancement ratio  $\zeta$  positively. The plot compares the Sobol First-order indices (S1), Total-order indices (ST), and Pearson correlation coefficients for multiple parameters, indicating their significance and effect size on  $\zeta$  (Color figure online)

Since the fluctuation of  $\zeta$  plays a crucial role in determining whether the situation is disease-infused or disease-free, it is important to understand the role of the involved parameters on the output variance of  $\zeta$ . We use Sobol sensitivity analysis as a method for global sensitivity analysis of  $\zeta$ . This method calculates the First-order indices (S1), which indicate the contribution to the output variance individually, and the Total-order indices (ST) which measure the total effect of each input parameter, including interactions with other parameters. Additionally, the Pearson correlation coefficient is calculated to understand how each input parameter affects the output  $\zeta$ , whether positively or negatively. This helps us gauge the strength and direction of the relationships between inputs and outputs. We generate the Fig. 3 using the eq. (5) and the input ranges obtained from Table 1 in the Appendix D.

With high Sobol indices and strongly negative correlations, it is clear that  $r$  and  $K$  are the most influential parameters (see Fig. 3). Other negatively correlated parameters  $\phi$  and  $\mu$  have minimal effects, while the recovery rate of symptomatic infected individuals  $\rho$  has a moderate impact. Among the positively impacting parameters,  $\eta_u$ ,  $\eta_r$ ,  $\sigma$ , and  $\beta_e$ , the ingestion rate of *Vibrio cholerae* from the environment ( $\beta_e$ ) and the shedding rate of symptomatic infected individuals ( $\eta_r$ ) have notable impacts on the output variance of  $\zeta$ . Our concern is to reduce the positive impact of  $\eta_u$ ,  $\eta_r$ , and  $\beta_e$  through intervention strategies, while all other parameters are fixed based on the infected region. The interventions-mediated pathogen enhancement ratio, which we call the controlled pathogen enhancement ratio ( $\zeta_c$ ), in its original terms is:

$$\zeta_c = \left[ \frac{(1 - \sigma)(1 - c_{fu})\eta_u}{\phi + \mu} + \frac{\sigma(1 - c_{fr})\eta_r}{\rho + \mu} \right] \times \frac{\mu N}{r_1 K} \times \frac{(1 - c_s)(1 - c_h)\beta_e}{(1 - c_s)(1 - c_h)\beta_e + v + \mu}. \tag{6}$$

The impacts of shedding rate-related terms are influenced by compliance with safe fecal disposal, while bacteria ingestion rate-related terms are controlled by compliance with water and food sanitation, handwashing, and vaccination.

## 2.2 Intervention Analyses

Cholera predominantly affects underdeveloped and developing countries, where it is not feasible to implement all the recommended interventions due to the requirement of substantial resources and financial investments. Therefore, our objective is to identify a pair of interventions that authorities can prioritize to reduce the surge in cholera transmission peak. Moreover, it is important to achieve a sufficient reduction in the pathogen enhancement ratio  $\zeta$  to approach a cholera-free state in the long run. To achieve this, first, we assess the level of population compliance needed to reduce the pathogen enhancement ratio when these interventions are implemented in pairs. This analysis is conducted in two parts: the first part explores scenarios without vaccination, and the second part examines the impact of including vaccination as an intervention. The reduction process involves targeting a specific pair of interventions at varying compliance levels while keeping other interventions fixed at either low or high compliance levels. By doing so, we can observe the required compliance levels for the targeted interventions to reduce  $\zeta_c$  effectively.

In panel (a) of Fig. 4, we examine how varying the compliance with safe fecal disposal by inapparent infected ( $c_{f_u}$ ) and reported infected ( $c_{f_r}$ ) affects  $\zeta_c$  while holding other intervention compliance levels constant. The results from the first row suggest that maintaining a high level of compliance in reported individuals ( $c_{f_r}$ ) is essential to reduce  $\zeta_c$  significantly, regardless of the compliance level in inapparent individuals ( $c_{f_u}$ ). However, increasing  $c_{f_u}$  linearly reduces the burden on  $c_{f_r}$ . The magnitude of this reduction depends on the difference in the shedding rate between the inapparent and reported groups. One important observation is that, with the introduction of vaccination, achieving a high level of compliance with safe fecal disposal among reported individuals ( $c_{f_r}$ ) leads to a greater reduction in the critical threshold  $\zeta_c$  compared to the scenario without vaccination.

In panel (b), we considered the variation in water and food sanitation compliance ( $c_s$ ) and handwashing compliance ( $c_h$ ) controlling  $\beta_e$ . Both compliance levels need to be very high to reduce  $\zeta_c$  in the absence of vaccination. However, the pressure on these two factors is greatly alleviated when vaccination is introduced.

In panel (c), we focused on varying  $c_s$  and  $c_{f_r}$ . Without vaccination, high  $c_{f_r}$  is favored for effectively reducing  $\zeta_c$ . As with the previous scenarios, the introduction of vaccination improves the situation, allowing both  $c_s$  and  $c_{f_r}$  to be around medium levels to achieve a reduced  $\zeta_c$ .

The analyses reveal that high compliance with safe fecal disposal among reported infected individuals has the greatest impact on reducing the pathogen enhancement ratio when considered alongside other interventions, without vaccination. This step implicitly controls the ingestion quantity of *Vibrio cholerae* by reducing the addition of bacteria to the reservoirs. Meanwhile, strict compliance with water and food sanitation

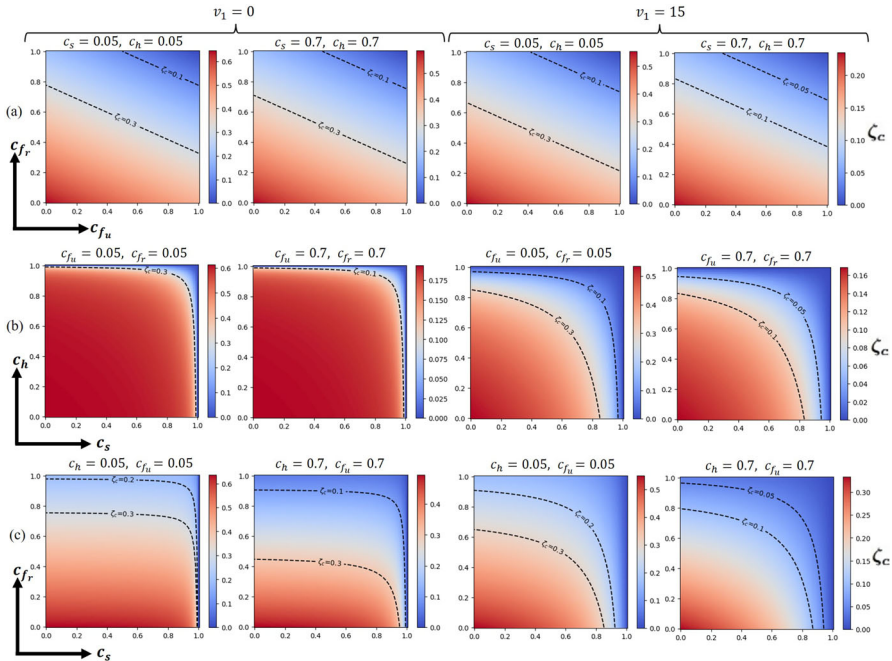


**Fig. 4** The dynamics of controlled pathogen enhancement ratio  $\zeta_c$ . To achieve a significant reduction in  $\zeta_c$  without vaccination: **(a)** In  $c_{f_u}$  vs  $c_{f_r}$  graph:  $c_{f_r}$  must remain high while increasing  $c_{f_u}$  linearly reduces the pressure on  $c_{f_r}$ , **(b)** In  $c_s$  vs  $c_h$  graph: Both parameters require to be very high and they directly reduce the individual level of infection, **(c)** In  $c_s$  vs  $c_{f_r}$  graph:  $c_{f_r}$  needs to be high, though very high  $c_s$  can alleviate the pressure on  $c_{f_r}$  in reducing  $\zeta_c$ . With vaccination, the parameter pairs interact more cooperatively to further reduce  $\zeta_c$  (Color figure online)

and handwashing are necessary for susceptible individuals to reduce the pathogen enhancement ratio. These measures directly affect the ingestion rate of *Vibrio cholerae* from the reservoir, thereby reducing cholera transmission. However, the introduction of vaccination eases the reliance on these interventions, allowing for more flexibility in compliance levels while still achieving significant reductions in  $\zeta_c$ .

To determine the most effective pair of interventions in reducing the peak of the cholera-infected population, we generate a figure that highlights the set creating the least average peak size of the reported infected population when a certain (MID, Level of Compliance) coordinate is chosen. The peak size refers to the maximum number of reported infections during the outbreak over a time period. Since the set that results in the smallest peak size varies based on the relationship between MID and the initial bacteria population, for each fixed pair of (MID, Compliance Level), the set that produces the lowest average peak size is determined by calculating the average peak size for each set over a range of initial bacteria population values. The lowest average providing set's corresponding color is then plotted as a tiny square in the MID vs Level of Compliance graph. The abruptness noticed in the plotting is attributed to this square shape. Note that each set is defined by selecting a specific pair of interventions (mentioned on the right side of each bar corresponding to the

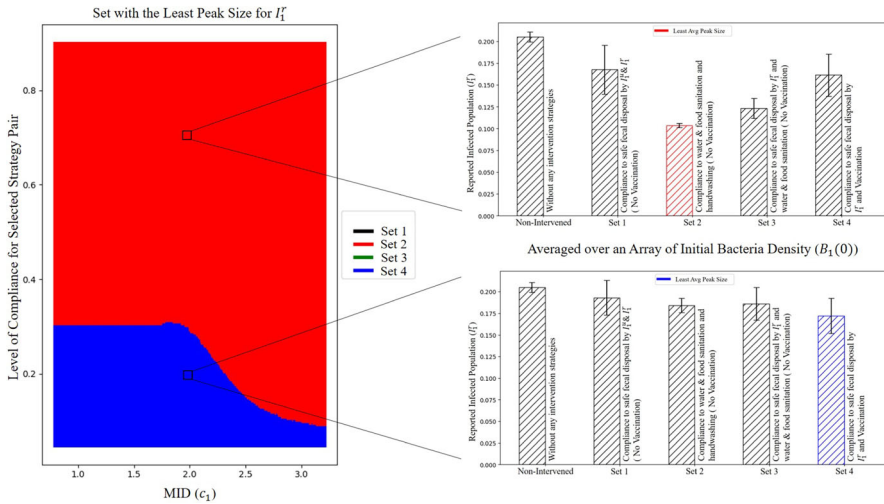


**Fig. 5** Selecting intervention pairs with the most reduced peak size of the reported infected population. Here, the compliance level for intervention strategies other than the selected pair is set at 0.05 (For example, with chosen compliance level of 70%, Set 1- where the selected pair for varied compliance is  $c_{f_r}$  and  $c_{f_u}$  -contains the values  $c_{f_u} = 0.7, c_{f_r} = 0.7$  while  $c_s = 0.05, c_h = 0.05$ ) and vaccination is adjusted to cover 15% of the susceptible population in 30 weeks if included (Color figure online)

set), for which compliance levels are varied, while the other interventions in that set are fixed at a very low compliance level of 0.05 (5%). This setup facilitates the identification of the most impactful combination of strategies in reducing the peak size under various situations. From the analysis illustrated in Fig. 5, combining water and food sanitation with handwashing proves to be the most effective pair at reducing reported cholera infections. Compared to other intervention pairs, this combination consistently reduces the peak size of reported cases most if the compliance level for the selected interventions is set at 32% or higher. However, for compliance levels lower than that the combination of safe fecal disposal of the reported infected population and high vaccination dominates in reducing the peak size. Here we define compliance level 32% or higher as moderate and high compliance, and below that as low compliance (following the percentage in Jobse et al. (2015)). A similar trend is observed for inapparent cholera cases too (see Fig. 15 in Appendix C). Overall, a reduction in the peak size is expected to provide a window for authorities to improve medical and other interventions.

### 3 Application: Cholera Transmission in Multiple Countries

To verify the validity of the model to real-world cholera outbreaks, we compiled the cholera case count data for several countries (Haiti, Kenya, Malawi, and Zimbabwe Africa Centres for Disease Control and Prevention (2024); Pan American Health Organization (2024); Rinaldo et al. (2012)) and used them to fit to the model. In particular, the case count data for the *V. cholerae* outbreak in Haiti from 2010 to 2011 was

adapted from Rinaldo et al. (2012) Rinaldo et al. (2012), while a more recent outbreak in Haiti (from October 2022 to March 2023) was adapted from the Pan American Health Organization (PAHO) (Pan American Health Organization 2024). Meanwhile, the case count data for Kenya, Malawi and Zimbabwe was compiled from January 2023 to May 2024 from the weekly surveillance reports provided by the Africa Centres for Disease Control and Prevention (Africa CDC) (Africa Centres for Disease Control and Prevention 2024). Since our model clearly distinguishes between inapparent and reported cholera cases, we fit the solution curve for *reported* cholera infections to the cholera outbreak data from each country, using parameter values based on the ranges provided in Table 1 of the Appendix D.

To obtain an optimal model fit, we used least-squares fitting techniques using the Cholera outbreak model in (1), and took  $c_s = 0$ ,  $c_h = 0$ ,  $c_{f_u} = 0$ ,  $c_{f_r} = 0$  and  $\nu = 0$  since we assume a negligible level of control measures being implemented in the isolated and impoverished communities most vulnerable to cholera (Amisu et al. 2024; Azevedo 2017; Kumar et al. 2022; Ngwa et al. 2017; Tappero and Tauxe 2011). We also take the recovery rate for inapparent cases to be based on the asymptomatic and symptomatic ranges mentioned in Table 1, ensuring that it equals or exceeds the recovery rate chosen for reported cases as established in the data fitting by Miller Neilan et al. (2004). We further take the mortality parameter  $\mu = \frac{1}{\text{Life expectancy} * 52.1}$  for each country, with the life expectancy data given by the World Health Organization (WHO) (World Health Organization Data 2024). Furthermore, since several of the outbreaks studied did not begin reporting their case counts until an outbreak was well underway (as evidenced by large initial case counts), the fits were also tested with a ‘burn-in’ period as needed, which was also estimated using least-squares fitting. This may be of use in estimating the beginning time of the outbreak.

To initialize the compartment values of the model fits, we took the total population  $N$  to denote all individuals who fail to comply with control measures (consistent with our assumption  $c_s = 0$ ,  $c_h = 0$ ,  $c_{f_u} = 0$ ,  $c_{f_r} = 0$ ) and who have no pre-existing immunity to cholera, given the model assumption that individuals with pre-existing immunity or who implement appropriate preventive measures are not susceptible to the cholera outbreak; since this population size  $N$  is influenced by multiple unknown environmental, demographic, cultural, and economic factors and hence cannot feasibly be estimated, we took an assumed  $N$ -value of approximately 10.5 – 13.5 times the cumulative recorded case count for each outbreak. Assuming that individuals who have recovered from previous cholera infection enjoy strong and long-term immunity (Harris 2018) and hence will not contribute to any further cholera outbreaks, we disregard any pre-existing members of the recovered compartment  $R(t)$  and hence take the initial size to be  $R(0) = 0$ . Meanwhile, the initial value for the reported infected compartment  $I^r(t)$  was taken to be  $I^r(0) = I_0$  (the first reported weekly case count) for outbreaks with no burn-in time, and  $I^r(0) = 1$  for outbreaks with a burn-in time and unknown initial case count. On the other hand, the initial size of the unreported compartment  $I^u(t)$  is taken to be  $I^u(0) = \frac{(1-\sigma)I^r(0)}{\sigma}$ , where the value of the (constant) reporting rate  $\sigma$  is estimated using least squares fitting of the weekly case data from each outbreak. By extension, the initial value of the susceptible compartment is taken to be  $S(0) = N - I^r(0) - I^u(0)$ . Finally, the initial value of the Bacteria compartment  $B(0)$  is taken to be slightly greater than the minimum infectious dose

(MID), in order for indirect transmission to commence in the population. It should be noted that including an original recovered compartment  $R(0) = R'$  in the overall population (yielding  $N' = N + R'$ ) will not impact the model fits and overall trends, as this initial recovered compartment does not interact with the outbreak (given their pre-existing immunity). Furthermore, our simulations indicate that the model trends are resilient to changes in the initialization of the reported compartment  $I^r(t)$ , since bacterial levels, instead of initial case counts, are predominantly responsible for the early spread of the disease in the susceptible population.

To verify the quality of the model fits to each of the outbreaks, we also fitted two other curves, given in Eqs. 7 and 8, to the weekly case data, and compared the resulting coefficients of determination  $R^2$  for each of these curves to our model fits; it should be noted that Eqs. 7 and 8 below were selected since they replicate the case count trends relatively well, for some constants  $a, b, c, d, e, f$ , and  $g$ .

$$f(t) = \frac{c}{a\sqrt{2\pi}} * e^{-\frac{1}{2}\left(\frac{t-b}{a}\right)^2} \tag{7}$$

$$g(t) = \frac{c}{d(t-g)^4 + e(t-g) + f} \tag{8}$$

Fitting the data for the 2010-2011 Cholera outbreak in Haiti (Rinaldo et al. 2012) yielded the weekly and cumulative case plots in Fig. 6, respectively. The fit yielded a mean reporting rate estimate of  $\sigma \approx 0.0921$  with standard deviation of approximately 0.00129, while the shedding ratio was estimated to be approximately 20.241 with standard deviation of 0.353 and the burn-in time was estimated to be 9 weeks. The weekly case plot in Fig. 6 yielded a corresponding coefficient of determination of  $R_{weekly}^2 \approx 0.7786$ , while fitting Eqs. 7 and 8 yielded  $R_f^2 \approx 0.7174$  and  $R_g^2 \approx 0.7636$ , respectively. Meanwhile, fitting the data for the 2022-2023 Cholera outbreak in Haiti (Pan American Health Organization 2024) yielded the weekly and cumulative case plots in Fig. 7, respectively, with an estimated reporting rate of  $\sigma \approx 0.1077$  with standard deviation of approximately 0.000722, as well as a mean shedding ratio of approximately 45.375 with standard deviation 0.1768. The weekly case plot in Fig. 7 yielded a corresponding coefficient of determination of  $R_{weekly}^2 \approx 0.8756$ , while fitting Eqs. 7 and 8 yielded  $R_f^2 \approx 0.5444$  and  $R_g^2 \approx 0.8548$ , respectively.

Thirdly, fitting the model to the weekly recorded cases from the Kenya outbreak (Africa Centres for Disease Control and Prevention 2024) yielded a mean reporting rate estimate of  $\sigma \approx 0.1147$  with standard deviation of approximately 0.001677, while the mean shedding ratio is approximately 48.50 with standard deviation of approximately 0.3536 and the estimated burn-in time is 11 weeks. However, the Kenya outbreak contained several weeks of missing case data which negatively impacted the cumulative model fit; to overcome this, we estimated the missing weekly case counts using linear interpolation, and included the weekly and estimated cumulative case

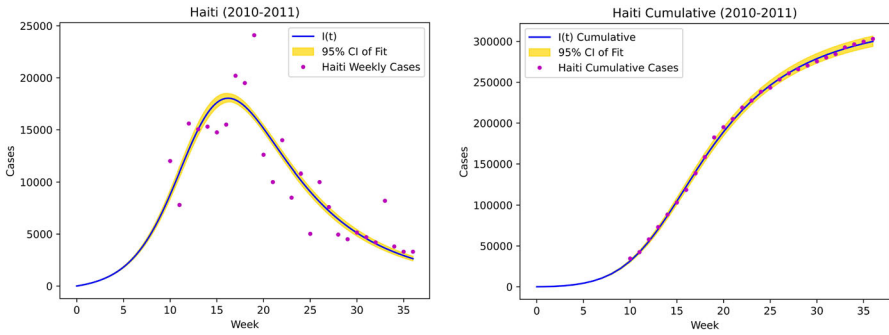


**Fig. 6** Weekly and cumulative model plots for the 2010-2011 Cholera outbreak in Haiti ( $R^2_{weekly} \approx 0.7786$  and  $R^2_{cumul} \approx 0.9988$ , respectively), with estimated reporting ratio  $\sigma \approx 0.0921$  and reported cases' shedding rate of approximately 20.241 times greater than inapparent cases. The inapparent infection recovery rate per day is  $\phi \approx 0.143$  and the corresponding inapparent shedding rate is  $\eta_u \approx 0.444$  (Color figure online)

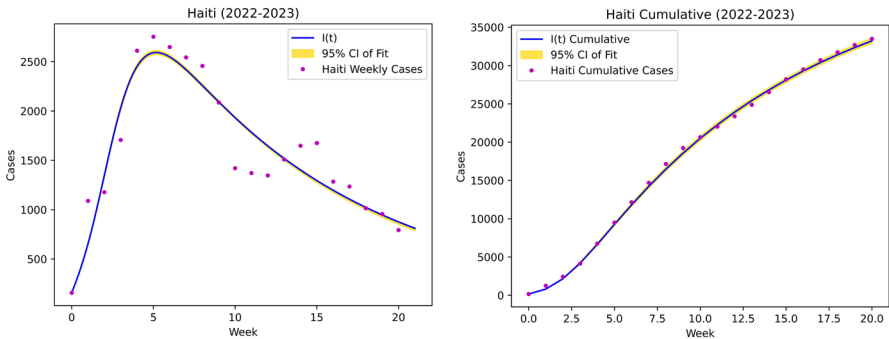


**Fig. 7** Weekly and cumulative model plots for the 2022-2023 Cholera outbreak in Haiti ( $R^2_{weekly} \approx 0.8756$  and  $R^2_{cumul} \approx 0.9989$ , respectively), with estimated reporting ratio  $\sigma \approx 0.1077$  and reported cases' shedding rate of approximately 45.375 times greater than inapparent cases. The inapparent infection recovery rate per day is  $\phi \approx 0.214$  and the corresponding inapparent shedding rate is  $\eta_u \approx 0.264$  (Color figure online)

plots in Fig. 16 in Appendix E, with the estimated missing data distinctly labeled in the cumulative plot. The weekly case plot in Fig. 16 yielded a corresponding coefficient of determination of  $R^2_{weekly} \approx 0.49210$ , while fitting Eqs. 7 and 8 yielded  $R^2_f \approx 0.49206$  and  $R^2_g \approx 0.48465$ , respectively.

Fourthly, fitting the model to the weekly recorded case data from the Malawi outbreak (Africa Centres for Disease Control and Prevention 2024) yielded the weekly and cumulative case plots in Fig. 8, respectively. The fit yielded a mean reporting rate estimate of  $\sigma \approx 0.0836$  with standard deviation of approximately 0.00096, while the mean shedding ratio was approximately 10.501 with standard deviation approximately 0.3509 and the estimated burn-in time was 9 weeks. The weekly case plot in Fig. 8 yielded a corresponding coefficient of determination of  $R^2_{weekly} \approx 0.9614$ , while fitting Eqs. 7 and 8 yielded  $R^2_f \approx 0.9585$  and  $R^2_g \approx 0.9594$ , respectively.

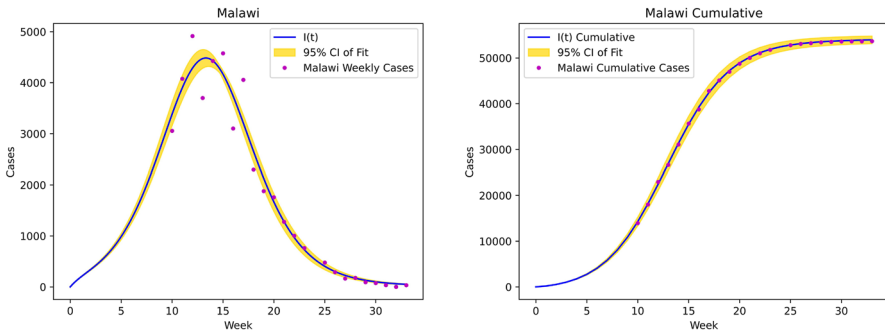


**Fig. 8** Weekly and cumulative model plots for the Cholera outbreak in Malawi ( $R^2_{weekly} \approx 0.9614$  and  $R^2_{cumul} \approx 0.9996$ , respectively), with estimated reporting ratio  $\sigma \approx 0.0836$  and reported cases’ shedding rate of approximately 10.501 times greater than inapparent cases. The inapparent infection recovery rate per day is  $\phi \approx 0.143$  and the corresponding inapparent shedding rate is  $\eta_u \approx 0.667$  (Color figure online)

Finally, fitting the model to the weekly recorded case data from the Zimbabwe outbreak (Africa Centres for Disease Control and Prevention 2024) using least-squares fitting yielded the weekly and cumulative case plots in Fig. 9, respectively. In this case, the estimated reporting rate was  $\sigma \approx 0.09425$  with standard deviation of approximately 0.001576, while the mean shedding ratio was approximately 24.75 with standard deviation approximately 0.0707. The weekly case plot in Fig. 9 yielded a corresponding coefficient of determination of  $R^2_{weekly} \approx 0.8364$ , while fitting Eqs. 7 and 8 yielded  $R^2_f \approx 0.8374$  and  $R^2_g \approx 0.8217$ , respectively. In all, the fitting results and estimated parameters in Figs. 6, 7, 8, 9, and 16 are consistent with the approximate severity rate and shedding rates outlined by Centers for Disease Control and Prevention (2024b); Chao et al. (2011); Miller Neilan et al. (2004), and the corresponding coefficients of determination  $R^2_{weekly}$  indicate that our model fits are (almost exclusively) superior to fitting the data using Eqs. 7 and 8. The graphical fits of the Cholera Model (1) and Eqs. 7 and 8, as well as their corresponding coefficients of determination  $R^2$ , are given in Appendix F.

We also record and compare the final cumulative number of reported and total (reported plus inapparent) cases estimated by the model fits for Haiti (Pan American Health Organization 2024; Rinaldo et al. 2012), Kenya, Malawi, and Zimbabwe (Africa Centres for Disease Control and Prevention 2024). It should be noted that, in cases of missing reporting data at the beginning of (or during) the outbreak, the estimated number of reported cases may exceed the recorded number. In particular, the model fit for the 2010-2011 outbreak in Haiti estimated a cumulative number of approximately 299, 946 recorded and 3, 260, 285 total cases. Meanwhile, the model fit for the 2022-2023 outbreak in Haiti estimated a cumulative number of approximately 34, 029 recorded and 241, 396 total cases. The lowest estimated case counts came from the model fit for Kenya, which estimated a cumulative number of approximately 12, 100 recorded and 100, 573 total cases. Furthermore, the model fit for Malawi estimated a cumulative number of approximately 53, 956 recorded and 467, 351 total cases. Finally, the model fit for Zimbabwe estimated a cumulative number of approx-

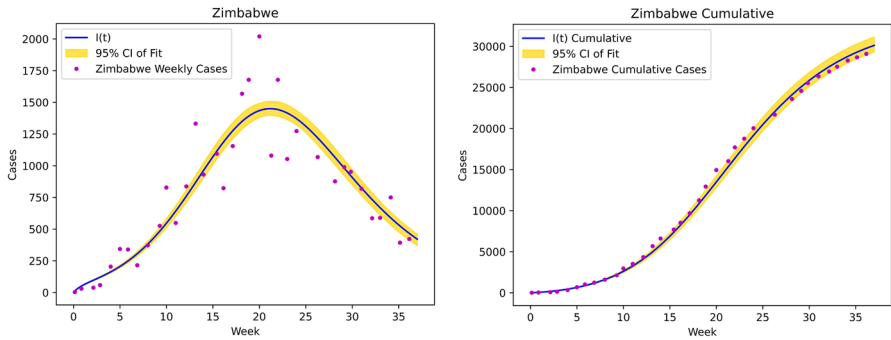


**Fig. 9** Weekly and cumulative model plots for the Cholera outbreak in Zimbabwe ( $R^2_{weekly} \approx 0.8364$  and  $R^2_{cumul} \approx 0.9950$ , respectively), with estimated reporting ratio  $\sigma \approx 0.09425$  and reported cases' shedding rate of approximately 24.75 times greater than inapparent cases. The inapparent infection recovery rate per day is  $\phi \approx 0.143$  and the corresponding inapparent shedding rate is  $\eta_u \approx 0.182$  (Color figure online)

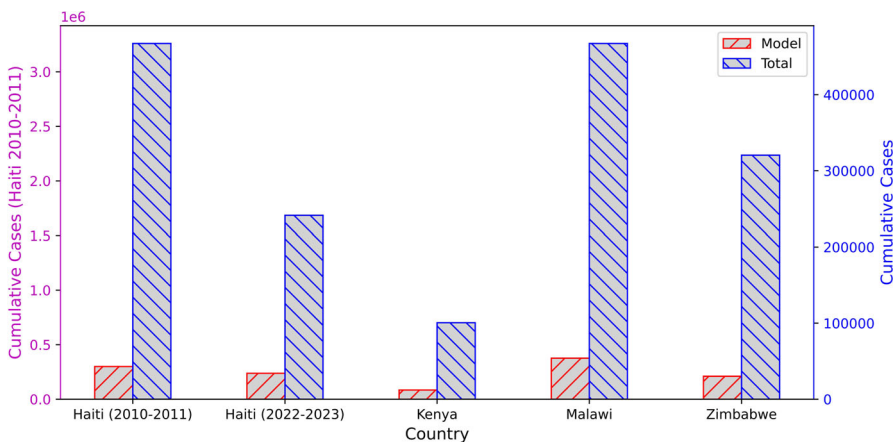


**Fig. 10** Estimated cumulative case counts. Haiti (2010-2011): 299,946 recorded and 3,260,285 total. Haiti (2022-2023): 34,029 recorded and 241,396 total. Kenya: 12,100 recorded and 100,573 total. Malawi: 53,956 recorded and 467,351 total. Zimbabwe: 30,120 recorded and 320,429 total (Color figure online)

imately 30, 120 recorded and 320, 429 total cases. The cumulative case counts for Haiti (2010-2011 and 2022-2023), Kenya, Malawi, and Zimbabwe are summarized in the bar chart in Fig. 10.

### 3.1 Testing Control Measures

Now that we have obtained a least-squares model fit to the reported data for the 2010-2011 and 2022-2023 Cholera outbreaks in Haiti (Rinaldo et al. 2012; Pan American Health Organization 2024) as well as for Kenya, Malawi, and Zimbabwe Africa Centres for Disease Control and Prevention (2024), it is instructive to estimate how the implementation of various control measures would influence the spread of cholera in those outbreaks. In situations of limited resources where not all control measures can

be effectively implemented simultaneously, this analysis could help evaluate which control measures should be prioritized.

The effectiveness of several control measures are studied in these outbreaks, including proper water/food sanitation, handwashing, safe fecal disposal, and vaccination. In particular, we analyze several combinations of these control measures: (1) water/food sanitation and handwashing; (2) water/food sanitation and safe fecal disposal for reported cases; (3) safe fecal disposal for reported cases and vaccination; and (4) safe fecal disposal for both reported and inapparent cases.

To gauge the effectiveness of these control measures, we elected to take a compliance level of 70% with regards to the selected combination of non-pharmaceutical control measures, and a baseline of 5% compliance for remaining measures. Meanwhile, assuming that a vaccination campaign would achieve 15% vaccination in the susceptible population over an outbreak period of approximately 30 weeks, we take the vaccination rate per week to be  $\nu = \frac{0.15}{30} = 0.005$  (or 0.5%).

Plotting the four control measure combinations and base case model fits for the 2010-2011 and the 2022-2023 Cholera outbreaks in Haiti (Rinaldo et al. 2012; Pan American Health Organization 2024) as well as the Malawi and Zimbabwe outbreaks (Africa Centres for Disease Control and Prevention 2024) yields Fig. 11, while plotting the effects of these control measures for the Kenya outbreak are given in Fig. 16 in Appendix E. As may be observed in the outbreaks depicted in Figs. 11 and 16, the most effective combination of control measures (in terms of reducing and delaying the peak of the outbreak as well as reducing cumulative case counts) is safe water/food sanitation and handwashing. On the other hand, the control measures of safe fecal disposal and vaccination proved to be least effective in reducing the spread of cholera in these outbreaks. These results match the conclusions of Wang & Wang (2015), who point out the relative ineffectiveness of vaccination in high bacterial growth scenarios and the importance of infrastructure development and water sanitation as a primary means of limiting cholera (Wang and Wang 2015).

Overall, the results of Fig. 11 clearly support prioritizing the non-pharmaceutical control measures of safe water/food sanitation and handwashing as the most effective means of slowing down and reducing the spread of cholera outbreaks.

## 4 Discussion

Despite cholera posing a significant threat to public health, many regions continue to neglect the necessary prevention measures (Akel et al. 2023; Orimbo et al. 2020). Unreported asymptomatic, underreported symptomatic, and reported symptomatic cholera cases in these regions further contaminate reservoirs with varying levels of *Vibrio cholerae* bacteria. In this study, we proposed an extension to Joh et al.'s (2009) basic iSIR model (Joh et al. 2009) to include inapparent infection, vaccination, and compliance levels for multiple non-pharmaceutical intervention strategies against cholera. In particular, compliance with non-pharmaceutical intervention strategies such as water and food sanitation and handwashing aimed to reduce the ingestion rates of *Vibrio cholerae*, thereby limiting transmission, while safe fecal disposal reduced the level of contamination of environmental reservoirs by bacteria shed from infected individuals.

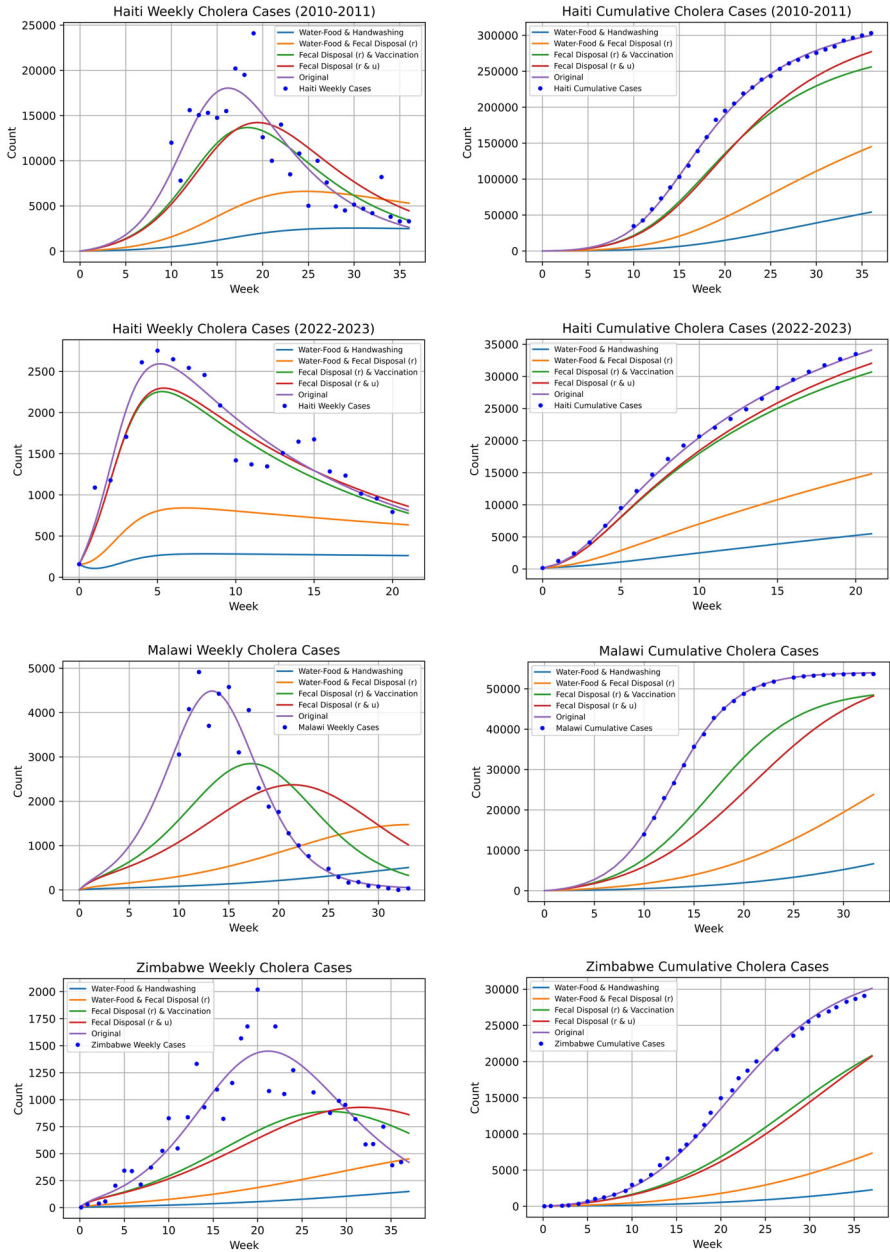


**Fig. 11** Testing the effectiveness of pairs of control measures on reducing cholera spread for Haiti, Malawi and Zimbabwe outbreaks, taking 70% compliance and 0.5% vaccination rate per week. Water/food sanitation and handwashing are the most effective pair of control measures in both weekly case fits (left) and cumulative case trajectories (right). Here,  $r$  and  $u$  in the legends represent reported and inapparent, respectively (Color figure online)

Additionally, vaccination enhanced the protection of susceptible individuals against cholera, reduced the size of the Susceptible compartment, and consequently lowered the impact of the ingestion rate on the pathogen enhancement ratio. It should be noted that we maintained Joh et al.'s (2009) (Joh et al. 2009) emphasis on the incorporation of a minimum infectious dose required for the spread of infection in our  $iSI^uI'R$  model. Numerical simulations of the model showed that when sufficient shedding contribution from inapparent infected individuals is added to that of reported infected people, the *Vibrio cholerae* density surged, and consequently it amplified the spread of the disease significantly. The equilibria and stability analyses (shown in Appendix B) of the model entailed that the preferable approach is to achieve a sufficiently small pathogen enhancement ratio to obtain a disease-free situation in the long run. The global sensitivity analysis of the pathogen enhancement ratio highlights the need to reduce the ingestion rate of *Vibrio cholerae* from the reservoir by the susceptible individuals and to increase safe fecal disposal by infected individuals to reduce the enhancement ratio.

Now, considering the need to limit the financial burden on developing countries of implementing all considered cholera intervention strategies, we further investigated which pair of interventions would prove most effective at reducing cholera infection curve peak sizes. In this case, compliance with water and food sanitation and hand-washing was found to be the most effective combination in significantly reducing the peak size of infection; this is because these intervention strategies directly limit the spread of infection on an individual level, provided that the people's compliance to these selected intervention strategies are at a moderate or high level ( $\geq 32\%$ ). Otherwise, if people have a low tendency to follow the interventions, then the combination of targeting safe fecal disposal among the reported infected population and conducting a high vaccination campaign for the susceptible population can most effectively reduce the peak size.

To verify the validity of the model to real-world epidemics, we fitted the model to the cholera outbreak data recorded from three African countries (Kenya, Malawi, Zimbabwe) (Africa Centres for Disease Control and Prevention 2024) and one Caribbean country (Haiti) (Pan American Health Organization 2024; Rinaldo et al. 2012), yielding Figs. 6, 7, 8, 9, 11, and 16. Our model fitting results indicate that up to 91.6% of infections are unreported or inapparent, while the shedding rate ratio between reported and inapparent infected individuals ranges from approximately 10.50 to 48.50. In situations where case data was only available after the outbreak was well underway, the model fit estimated a burn-in time of as much as 11 weeks from the start of the outbreak until the commencement of reporting. Analyzing the effect of moderate to high compliance rates for the selected pairs of interventions while maintaining only 5% compliance for other measures, our fitting analysis identified that water/food sanitation and handwashing were unequivocally the most effective control measures in reducing the spread of cholera. This finding aligns with observations by Andrews and Basu (2011), who reported that the use of clean water had the strongest impact on reducing cases and mortality during the cholera outbreak in Haiti (Andrews and Basu 2011). The overall effectiveness of non-pharmaceutical interventions in controlling cholera spread is further supported by the Centres for Disease Control and Prevention, which note that the near-eradication of cholera in the United States was

achieved through the implementation of modern water and sewage sanitation systems (Centers for Disease Control and Prevention 2024a), not mass vaccination or other pharmaceutical interventions. In conclusion, our observations and results indicate that implementing water/food sanitation and handwashing is the most effective combination of intervention strategies and should be prioritized in cases of moderate or high compliance ( $\geq 32\%$ ) to most effectively limit the spread of cholera outbreaks.

One potential limitation of our work might be treating the asymptomatic and under-reported symptomatic people in a single compartment to facilitate the tractability of inapparent infections, intervention-focused analysis, and explicit reported data fitting, despite their differences in recovery and shedding rates. Several directions of further development of this model could be made, particularly in the setting of the minimum infectious dose. These include introducing a separate compartment for vaccinated individuals with waning immunity and adding a protected compartment for those who are wealthy and educated (susceptible but with a lower risk of exposure) (Ng’ Ombé et al. 2022; Dowling et al. 2013). In the current model, compliance is treated as a fixed parameter; however, it could be allowed to vary according to an evolutionary game theory approach, reflecting individual decisions based on payoffs. This would better capture the adaptive nature of human behavior, where people choose interventions based on perceived benefits (Alexander 2023). Also, adding a time delay for implementing the strategies and considering randomness in the data sets can be other directions of extension.

### Appendix A: Proof of Forward Invariance

From the first equation of the system 1,  $\dot{S}(S = 0) = \mu N > 0$ . Hence  $S(t) > 0$  for  $t > 0$ .

Now combining the fact that  $\alpha(B) \geq 0, v \geq 0$  and  $S(t) > 0$  we get,  $\dot{I}^u(I^u = 0) \geq 0, \dot{I}^r(I^r = 0) \geq 0$  and  $\dot{R}(R = 0) \geq 0$ . Thus,  $I^u(t) \geq 0, I^r(t) \geq 0$  and  $R(t) \geq 0$  for  $t > 0$ .

From the equation of *Vibrio cholera* density, we have  $\dot{B}(B = 0) = (1 - c_{f_u}) \eta_u I^u + (1 - c_{f_r}) \eta_r I^r \geq 0$ . So  $B(t) \geq 0$  with  $t > 0$ . Since  $S + I^u + I^r + R = N$ , with  $c_f = \min\{c_{f_u}, c_{f_r}\}$  and  $\eta = \max\{\eta_u, \eta_r\}$  the fifth equation of system 1 gives,

$$\dot{B} < r_1 B \left(1 - \frac{B}{K}\right) + (1 - c_f)\eta N = F(B).$$

Now from the roots of  $F(B) = 0$ , we can define  $B_{\max}$  as follows,

$$B_{\max} = \frac{Kr_1 + K\sqrt{r_1^2 + 4(1 - c_f)\frac{r_1\eta N}{K}}}{2r_1}$$

such that if  $B(0) \in [0, B_{\max})$  then  $B(t) \in [0, B_{\max})$  for  $t \geq 0$ .

### Appendix B: Equilibria and Stability Details

We use the non-dimensionalized model 3 to determine the equilibria and consider whether the transmissibility,  $\alpha_1(B_1)$ , is zero or non-zero. Also, the following results are derived without any intervention strategies i.e.  $c_s = 0; c_h = 0; v = 0; c_{f_u} = 0; c_{f_r} = 0$ .

When transmissibility is zero, disease-free equilibria are expected. The existence and number of equilibrium points depend on the rescaled minimum infectious dose (MID) value  $c_1$ . If  $c_1 < 1$ , meaning the MID does not exceed the bacterial carrying capacity in the environment, there is only one equilibrium point,  $E_1 = (S_1, I_1^u, I_1^r, B_1) = (1, 0, 0, 0)$ , which is a saddle point (see Fig. 13). Its stability property is identified from the Eigenvalues of the corresponding Jacobian, where

$$J(E_1) = \begin{pmatrix} -p_s & 0 & 0 & 0 \\ 0 & -p_u & 0 & 0 \\ 0 & 0 & -p_r & 0 \\ 0 & q_u & q_r & r_1 \end{pmatrix},$$

and the existence of the positive eigenvalue  $r_1$  makes the equilibrium  $E_1$  saddle, while other three  $-p_s, -p_u, -p_r$  are clearly negative. Conversely, if  $c_1 > 1$ , meaning the MID exceeds the bacterial carrying capacity, there is an additional stable equilibrium point,  $E_2 = (S_2, I_2^u, I_2^r, B_1) = (1, 0, 0, 1)$  (see Fig. 13 (b) & 13(c)). All eigenvalues of the corresponding Jacobian at  $E_2$  are negative, where

$$J(E_2) = \begin{pmatrix} -p_s & 0 & 0 & 0 \\ 0 & -p_u & 0 & 0 \\ 0 & 0 & -p_r & 0 \\ 0 & q_u & q_r & -r_1 \end{pmatrix},$$

With the non-zero transmissibility i.e.  $\alpha_1(B_1) = \frac{\beta(B_1 - c_1)}{(B_1 - c_1) + \lambda}$ , under the condition  $B_1^* > c_1$ , the equilibria appear to be of the form  $(S_1^*, A_1^*, I_1^*, B_1^*) = \left( \frac{1}{\alpha_1(B_1^*) + 1}, \frac{(1 - \sigma)p_r}{\sigma p_u} \times \frac{\tilde{r}_1 B_1^*(B_1^* - 1)}{q_u \frac{(1 - \sigma)p_r}{\sigma p_u} + q_r}, \frac{\tilde{r}_1 B_1^*(B_1^* - 1)}{q_u \frac{(1 - \sigma)p_r}{\sigma p_u} + q_r}, B_1^* \right)$  where  $B_1^*$  is obtained as roots of the the following equation:

$$B_1^*(B_1^* - 1) \left[ B_1^* - \left( c_1 - \frac{\lambda}{\beta + 1} \right) \right] = \zeta (B_1^* - c_1) \tag{9}$$

with

$$\zeta = \left[ \frac{(1 - \sigma)q_u}{\tilde{r}_1 p_u} + \frac{\sigma q_r}{\tilde{r}_1 p_r} \right] \times \frac{\beta}{\beta + 1}, \tag{10}$$

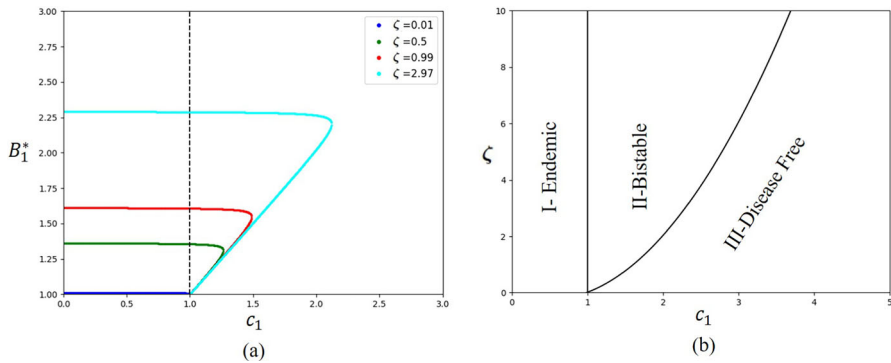


**Fig. 12** Absence of Saddle-Node bifurcation for sufficiently small  $\zeta$  with bifurcation parameter  $c_1$ . **(a)** The shift in the number of non-trivial equilibrium pathogen densities with  $B_1^* > c_1$  for various  $\zeta$ , using Eq. (9). **(b)** Showcase of stable states in a bifurcation diagram for  $\beta = 100$  and  $\lambda = 1$  (Color figure online)

and in original terms, it looks like the following:

$$\zeta = \left[ \frac{(1 - \sigma)\eta_u}{\phi + \mu} + \frac{\sigma\eta_r}{\rho + \mu} \right] \times \frac{\mu N}{r_1 K} \times \frac{\beta_e}{\beta_e + \mu}. \tag{11}$$

Which yields Eq. 5. The equilibrium points in this case are found by analyzing the roots of the Eq. (9). While every other parameter is fixed, the relationship between  $c_1$  and  $\zeta$  is significant in determining the number of equilibrium points. With  $c_1 < 1$ , there is always a root  $B_1^* > c_1$  of the Eq. (Fig. 12(a)) for any value of  $\zeta$  corresponding to a stable equilibrium  $E_1^* = (S_1^*, I_1^{u*}, I_1^{r*}, B_1^*)$  (Fig. 13(a)).

If  $c_1 > 1$ , the number of equilibrium points changes with the value of  $\zeta$  (Fig. 12). For a sufficiently small  $\zeta$  value, there is no equilibrium with  $B_1^* > c_1$  and the equilibrium  $E_2 = (1, 0, 0, 1)$  becomes stable (see Fig. 13 (c)). However, as the value of  $\zeta$  increases, two additional equilibria,  $E_3^* = (S_3^*, I_3^{u*}, I_3^{r*}, B_3^*)$  and  $E_4^* = (S_4^*, I_4^{u*}, I_4^{r*}, B_4^*)$  are created via saddle node bifurcation (Fig. 12). In this case, the equilibrium  $E_4^*$  is stable with  $I_4^{u*} > I_3^{u*}$ , while  $E_3^*$  a saddle point (Fig. 13(b)). Note that we couldn't prove the stability of non-trivial equilibrium  $E_1^*$ ,  $E_3^*$ , and  $E_4^*$  analytically, but the stability result is concluded based on the numerical results shown in Fig. 12 and 13.

We summarize the result in the following proposition.

**Proposition 2 (Equilibria)**

- (i) For  $c_1 < 1$ , two equilibria exist:  $E_1 = (1, 0, 0, 0)$  is saddle, while  $E_1^* = (S_1^*, I_1^{u*}, I_1^{r*}, B_1^*)$  is stable with  $I_1^{u*}, I_1^{r*} > 0$ . This implies that cholera becomes endemic in this scenario.
- (ii) For  $c_1 > 1$ , there always exist two equilibria:  $E_1 = (1, 0, 0, 0)$  which is a saddle point and  $E_2 = (1, 0, 0, 1)$ , which is stable. For sufficiently large values of  $\zeta$ , up to additional two equilibria can exist:  $E_3^* = (S_3^*, I_3^{u*}, I_3^{r*}, B_3^*)$ , a saddle point and  $E_4^* = (S_4^*, I_4^{u*}, I_4^{r*}, B_4^*)$  a stable point, where  $I_4^{u*} > I_3^{u*}$ . However, no additional equilibria exist for small enough  $\zeta$  values, and the disease-free state  $E_2 = (1, 0, 0, 1)$  becomes stable for almost every initial condition.

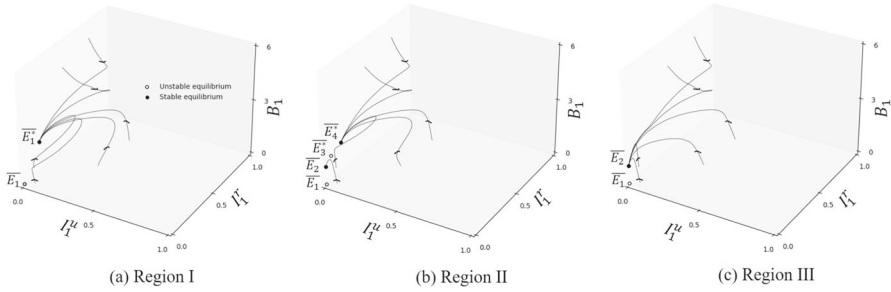


**Fig. 13** Schematic diagram of phase-portraits projected into  $I_1^u - I_1^i - B_1$  space. **(a)** Corresponding to the region I in Fig. 12**(b)**: the disease persists asymptotically where  $c_1 = 0.8 < 1, \zeta = 2.23$  **(b)** corresponding to region II: the situation is bistable i.e. most trajectories approach either disease-free (with bacteria at carrying capacity) or endemic situation where  $c_1 = 1.5, \zeta = 2.23$  **(c)** corresponding to region III: the infected cases approaches zero though bacteria survive at carrying capacity where  $c_1 = 2.5, \zeta = 2.23$  (Color figure online)

From the above analyses, it is evident that the rise and fall of  $\zeta$  play a crucial role in determining whether the situation is disease-infused or disease-free. According to Joh et al. (2009) (Joh et al. 2009),  $\zeta$  is referred to as the pathogen enhancement ratio.

### Appendix C

See Figs. 14 and 15.

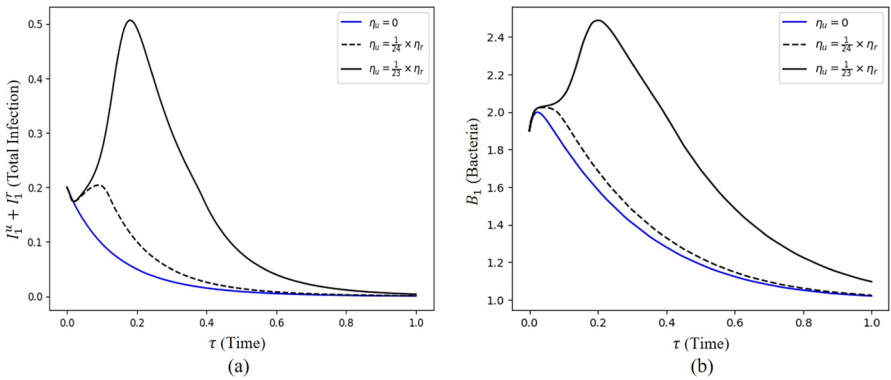


**Fig. 14** A large outbreak requiring sufficient shedding from inapparent infected. Here, **(a)** shows a significant rise in the total infection and **(b)** highlights the surge of *Vibrio cholera* density responsible for this increased infection. Parameters value used are  $c_s = 0.0, c_h = 0.0, v = 0.0, c_{fr} = 0.0 \beta = 100, c_1 = 2, p_s = 1, p_u = 10, p_r = 5, q_u = 0/18.75/19.57, q_r = 450$  (Color figure online)

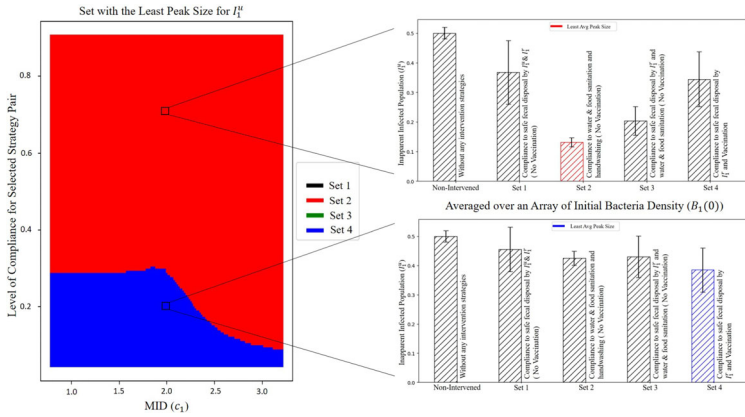


**Fig. 15** Selecting intervention pairs with the most reduced peak size of the inapparent infected population. Here, the compliance level for intervention strategies other than the selected pair is set at 0.05 ( For example, with chosen compliance level of 70%, Set 1- where the selected pair for varied compliance is  $c_{f_r}$  and  $c_{f_u}$  -contains the values  $c_{f_u} = 0.7, c_{f_r} = 0.7$  while  $c_s = 0.05, c_h = 0.05$  ) and vaccination is adjusted to cover 15% of the susceptible population in 30 weeks if included (Color figure online)

## Appendix D

See Table 1.

**Table 1** List of Parameters

Parameter	Symbol	Value/Range	Unit	Source
Pathogen carrying capacity	$K$	$10^2 - 10^4, 10^4 - 10^6$	Cells/mL	(Colwell et al. 1990; Jensen et al. 2006; Kong et al. 2014)
Half saturation pathogen density	$H$	$10^5 - 10^6$	Cells/mL	(Fung 2014; Hartley et al. 2006)
Total at-risk population	$N$			Changes country-wise
Minimum Infectious Dose (MID)	$c$	$10^3 - 10^6$	Cells/mL	(Colwell et al. 1996; Joh et al. 2009; Levine et al. 1981)
Ingestion rate of <i>Vibrio cholera</i> from the contaminated reservoir	$\beta_e$	$10^{-5} - 1, 1.869 \times 10^{-8}, 1.2667 \times \frac{10^{-6}}{7}$	Per day	(Bai et al. 2021; Che et al. 2021; Fung 2014)
Maximum per capita pathogen growth efficiency	$r$	$0.3 - 14.3$	Per day	(Jensen et al. 2006; Kong et al. 2014; Wang 2022)
Proportion of compliance with water and food sanitation among susceptible individuals	$c_s$	$0.0 - 1.0$		Assumed
Proportion of compliance with handwashing among susceptible individuals	$c_h$	$0.0 - 1.0$		Assumed
Proportion of compliance with safe fecal disposal by inapparent infected individuals	$c_{fu}$	$0.0 - 1.0$		Assumed
Proportion of compliance with safe fecal disposal by reported infected individuals	$c_{fr}$	$0.0 - 1.0$		Assumed
Vaccination rate among susceptible	$v$	$0.0 - 1.0$	Per day	Assumed
Reported fraction	$\sigma$	$0.0 - 1.0$		Fitted
Per capita human birth and death rate	$\mu$	$\frac{1}{365 \times LfI eSpan}$ or $\frac{1}{52.1 \times LfI eSpan}$	Per day/week	Changes country-wise
Inapparent infection recovery rate	$\phi$	$0.0 - 1.0$	Per day	Fitted
Reported infection recovery rate	$\rho$	$0.06, [0.07 - 0.2], [0.07 - 0.34]$	Per day	(Dangbé et al. 2018; Fung 2014; King et al. 2008)
Pathogen shedding ratio of reported to inapparent infected	$\frac{\eta_r}{\eta_u}$	$10 - 100$		Fitted
Pathogen shedding rate of reported infected	$\eta_r$	$0.01 - 10, 10^8$	Cells/mL/person/day	(Fung 2014; Hartley et al. 2006; Finkelstein 1996)

### Appendix E

Fitting the model to the weekly recorded cases from the Kenya outbreak (Africa Centres for Disease Control and Prevention 2024) yielded Fig. 16. The fits yielded a mean reporting rate estimate of  $\sigma \approx 0.1147$  with standard deviation of approximately 0.001677, while the mean shedding ratio is approximately 48.50 with standard deviation of approximately 0.3536 and an estimated burn-in time of 11 weeks; furthermore, the corresponding coefficient of variation is  $R^2 = 0.49210$ . The missing weekly case counts in the Kenya data were estimated using linear interpolation and used to estimate the cumulative case plots in the right-hand graphs of Fig. 16. The simulations also show that the control measure combination of food/water sanitation and handwashing is most effective in reducing and delaying the outbreak peak and limiting the cumulative case count.

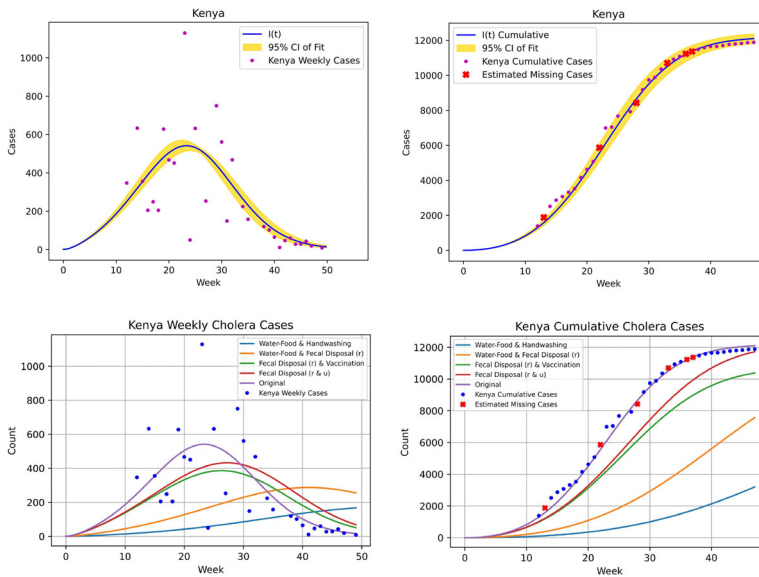


**Fig. 16** Weekly and cumulative model plots for the Cholera outbreak in Kenya ( $R^2_{weekly} \approx 0.49210$  and  $R^2_{cumul} \approx 0.99316$ , respectively), with estimated reporting ratio  $\sigma \approx 0.1147$  and reported cases' shedding rate of approximately 48.50 times greater than inapparent cases. The inapparent infection recovery rate per day is  $\phi \approx 0.143$  and the corresponding inapparent shedding rate is  $\eta_u \approx 0.0206$ . The missing weekly data was estimated using linear interpolation and included in the estimated cumulative curve to the right (Color figure online)

### Appendix F

To verify the goodness of fit of our model to the weekly case data for Haiti, Kenya, Malawi, and Zimbabwe (Africa Centres for Disease Control and Prevention 2024; Pan American Health Organization 2024; Rinaldo et al. 2012), we also fitted the data using Eqs. 7 and 8. The model fits for the Cholera model (1) and Eqs. 7 and 8, as well as their corresponding coefficients of determination  $R^2$ , are given in Fig. 17.

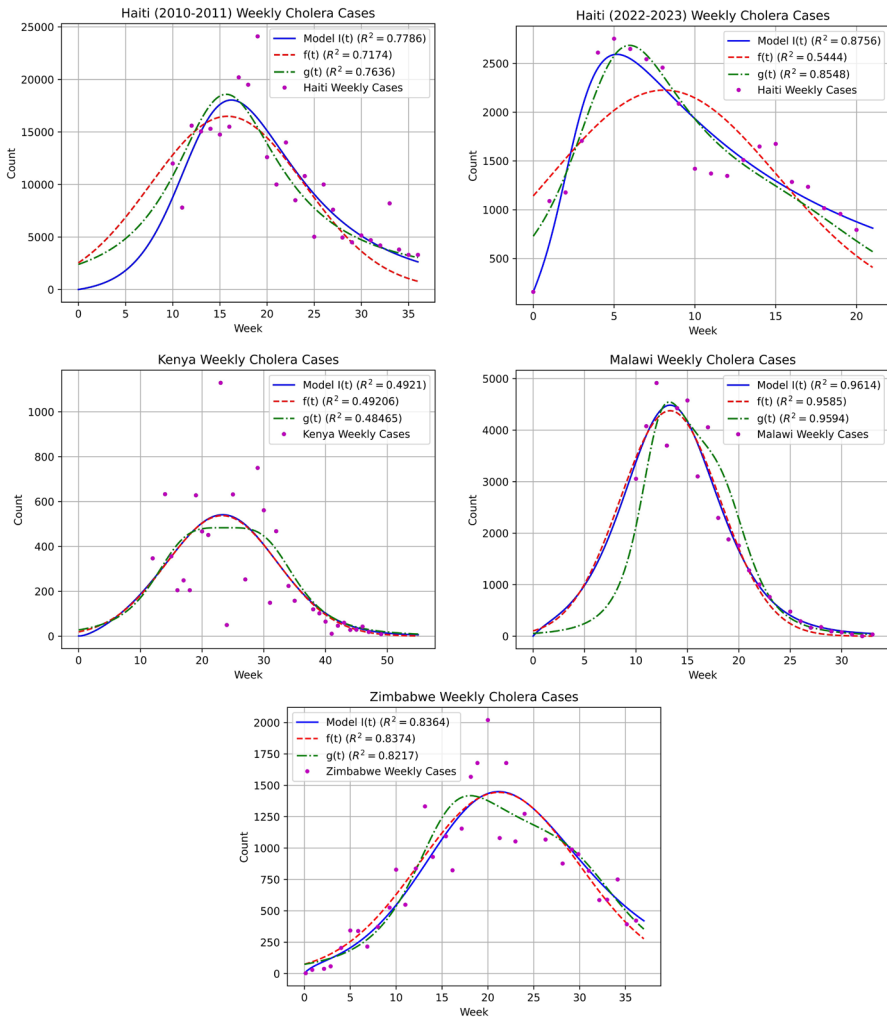


**Fig. 17** Plotting the Weekly case data for Haiti, Kenya, Malawi, and Zimbabwe (Africa Centres for Disease Control and Prevention 2024; Pan American Health Organization 2024; Rinaldo et al. 2012) versus the fits obtained using the Cholera outbreak model in (1) as well as Eqs. 7 and 8. The cholera model fits yield (almost exclusively) greater coefficients of variation  $R^2$  compared to Eqs. 7 and 8 (Color figure online)

**Acknowledgements** Hao Wang acknowledges the support from a Canada Research Chair and the Natural Sciences and Engineering Research Council of Canada (Individual Discovery Grant RGPIN-2020-03911 and Discovery Accelerator Supplement Award RGPAS-2020-00090). ChatGPT and QuillBot were used to polish writing.

**Data Availability** All data used in this paper were obtained from published papers or public sources.

## References

- Africa Centres for Disease Control and Prevention. Surveillance Archives. Retrieved May 21, 2024, from <https://africacdc.org/pillar/surveillance/>
- Marwan Akel, Fouad Sakr, Chadia Haddad, Aline Hajj, Hala Sacre, Zeenny Rony M, Jihan Safwan, Pascale Salameh (2023) Knowledge, attitude, and practices of the general population toward the old-new outbreak of cholera in a developing country. *Tropical Medicine and Infectious Disease* 8(4):236
- Alexander J McKenzie (2023) *Evolutionary game theory*. Cambridge University Press
- Mohammad Ali, Nelson Allyson R, Lena Lopez Anna, Sack David A (2015) Updated global burden of cholera in endemic countries. *PLoS neglected tropical diseases* 9(6):e0003832
- Amisu BO, Okesanya OJ, Adigun OA, Manirambona E, Ukoaka BM, Lawal OA, Idris NB, Olaleke NO, Okon II, Ogaya JB, Priso DEL (2024) 3rd . Cholera resurgence in africa: assessing progress, challenges, and public health response towards the 2030 global elimination target. *Le infezioni in medicina*, 32(2):148–156. <https://doi.org/10.53854/liim-3202-4>
- Andrews JR, Basu S (2011) Transmission dynamics and control of cholera in haiti: an epidemic model. *Lancet* 377(9773):1248–55. [https://doi.org/10.1016/S0140-6736\(11\)60273-0](https://doi.org/10.1016/S0140-6736(11)60273-0)
- Azevedo Mario J (2017) *The State of Health System(s) in Africa: Challenges and Opportunities*, pages 1–73. Springer International Publishing
- Bai Ning, Song Chenwei, Rui Xu (2021) Mathematical analysis and application of a cholera transmission model with waning vaccine-induced immunity. *Nonlinear Analysis: Real World Applications* 58:103232
- Bernoulli Daniel (1766) A new analysis of the mortality caused by smallpox. *Mem. Math. Phys. Acad. Roy. Sci. Paris*,
- Bertuzzo Enrico, Mari Lorenzo, Righetto L, Gatto Marino, Casagrandi Renato, Blokesch M, Rodriguez-Iturbe I, Rinaldo Andrea (2011) Prediction of the spatial evolution and effects of control measures for the unfolding haiti cholera outbreak. *Geophysical Research Letters*, 38(6)
- Centers for Disease Control and Prevention (2024) About Cholera in the United States. <https://www.cdc.gov/cholera/about/about-cholera-in-the-united-states.html> Accessed August 4
- Centers for Disease Control and Prevention (2024) Signs and symptoms of cholera. <https://www.cdc.gov/cholera/signs-symptoms/index.html> Accessed August 4
- Chao Dennis L, Elizabeth Halloran M, Longini Ira M, Jr (2011) Vaccination strategies for epidemic cholera in haiti with implications for the developing world. *PNAS*, 108(17):7081–85. <https://doi.org/10.1073/pnas.1102149108>
- Che Eric, Numfor Eric, Lenhart Suzanne, Yakubu Abdul-Aziz (2021) Mathematical modeling of the influence of cultural practices on cholera infections in cameroon. *Mathematical Biosciences and Engineering* 18(6):8374–8391
- Colwell RR, Brayton P, Herrington D, Tall B, Huq A, Levine MM (1996) Viable but non-culturable vibrio cholerae o1 revert to a cultivable state in the human intestine. *World Journal of Microbiology and Biotechnology* 12:28–31
- Colwell RR, Tamplin ML, Brayton PR, Gauzens AL, Tall BD, Herrington D, Levine MM, Hall S, Huq A, Sack DA (1990) Advances in research on cholera and related diarrhoea. 7th
- Conner Jenna G, Teschler Jennifer K, Jones Christopher J, Yildiz Fitnat H (2016) Staying alive: Vibrio cholerae's cycle of environmental survival, transmission, and dissemination. *Virulence mechanisms of bacterial pathogens*, pages 593–633
- Daley Daryl J, Gani Joseph Mark (1999) *Epidemic modelling: an introduction*. Number 15. Cambridge University Press
- Dangbé Ezekiel, Irépran Damakoa, Perasso Antoine, Békollé David (2018) Mathematical modelling and numerical simulations of the influence of hygiene and seasons on the spread of cholera. *Mathematical biosciences* 296:60–70

- Deen Jacqueline (2020) Martin A Mengel, and John D Clemens. Epidemiology of cholera. *Vaccine* 38:A31–A40. <https://doi.org/10.1016/j.vaccine.2019.07.078>
- Finkelstein Richard A (1996) Cholera, vibrio cholerae o1 and o139, and other pathogenic vibrios. *Medical Microbiology. 4th edition*
- Fung I C-H (2014) Cholera transmission dynamic models for public health practitioners. *Emerging Themes in Epidemiology*, 11(1). <https://doi.org/10.1186/1742-7622-11-1>
- Global Task Force on Cholera Control (GTFCC) (2017) Ending cholera: A global roadmap to 2030. <https://www.gtfcc.org/wp-content/uploads/2019/10/gtfcc-ending-cholera-a-global-roadmap-to-2030.pdf>. Accessed: 2024-08-28
- Harris Jason B (2018) Cholera: Immunity and prospects in vaccine development. *The Journal of Infectious Diseases*, 218(suppl3):141–146. <https://doi.org/10.1093/infdis/jiy414>
- Hartley David M, Morris Jr J Glenn, Smith David L (2006) Hyperinfectivity: a critical element in the ability of v. cholerae to cause epidemics? *PLoS medicine*, 3(1):e7
- Hegde Sonia T, Khan Ashraful Islam, Perez-Saez Javier, Khan Ishtiaqul Islam, Hulse Juan Dent, Islam Md Taufiqul, Khan Zahid Hasan, Ahmed Shakeel, Bertuna Taner, Rashid Mamunur et al (2024) Clinical surveillance systems obscure the true cholera infection burden in an endemic region. *Nature medicine* 30(3):888–895
- Hemson David, Dube Bongzi, Mbele Thami, Nnadozie Remigius, Ngcobo Dumisani (2006) *Still paying the price: revisiting the cholera epidemic of 2000-2001 in South Africa*. Municipal Services Projects
- Hethcote Herbert W (2000) The mathematics of infectious diseases. *SIAM review* 42(4):599–653
- Jensen Mark A, Faruque Shah M, Mekalanos John J, Levin Bruce R (2006) Modeling the role of bacteriophage in the control of cholera outbreaks. *Proceedings of the National Academy of Sciences* 103(12):4652–4657
- Inken Jobse, Liao Y, Bartram M, Delantonio K, Uter W, Stehle P, Sieber CC, Volkert D (2015) Compliance of nursing home residents with a nutrient-and energy-dense oral nutritional supplement determines effects on nutritional status. *The journal of nutrition, health & aging* 19:356–364
- Joh Richard I, Wang Hao, Weiss Howard, Weitz Joshua S (2009) Dynamics of indirectly transmitted infectious diseases with immunological threshold. *Bulletin of mathematical biology* 71:845–62. <https://doi.org/10.1007/s11538-008-9384-4>
- King Aaron A, Ionides Edward L, Pascual Mercedes, Bouma Menno J (2008) Inapparent infections and cholera dynamics. *Nature* 454:877–880. <https://doi.org/10.1038/nature07084>
- Kirpich Alexander, Weppelmann Thomas A, Yang Yang, Ali Afsar, Morris Jr J Glenn, Longini Ira M (2015) Cholera transmission in ouest department of haiti: dynamic modeling and the future of the epidemic. *PLoS neglected tropical diseases*, 9(10):e0004153
- Jude D Kong, William Davis, and Hao Wang (2014) Dynamics of a cholera transmission model with immunological threshold and natural phage control in reservoir. *Bulletin of mathematical biology*, 76(8):2025–2051
- Kumar A, Barve U, Gopalkrishna V, Tandale BV, Katendra S, Joshi MS, Salve D, Viswanathan R (2022) Outbreak of cholera in a remote village in western India. *The Indian journal of medical research* 156(3):442–448. [https://doi.org/10.4103/ijmr.IJMR\\_2440\\_20](https://doi.org/10.4103/ijmr.IJMR_2440_20)
- Lee Elizabeth C, Chao Dennis L, Lemaitre Joseph C, Matrajt Laura, Pasetto Damiano, Perez-Saez Javier, Finger Flavio, Rinaldo Andrea, Sugimoto Jonathan D, Elizabeth Halloran M et al (2020) Achieving coordinated national immunity and cholera elimination in haiti through vaccination: a modelling study. *The Lancet Global Health* 8(8):e1081–e1089
- MM Levine, RE Black, ML Clements, DR Nalin, L Cisneros, and RA Finkelstein (1981) Volunteer studies in development of vaccines against cholera and enterotoxigenic escherichia coli: a review. *Acute enteric infections in children. New prospects for treatment and prevention*, pages 443–459
- Longini Jr Ira M, Nizam Azhar, Ali Mohammad, Yunus Mohammad, Shenvi Neeta, Clemens John D (2007) Controlling endemic cholera with oral vaccines. *PLoS medicine*, 4(11):e336
- Mandal Shyamapada, Mandal Manisha Deb, Pal Nishith Kumar (2011) Cholera: a great global concern. *Asian Pacific Journal of Tropical Medicine*, 4(7):573–580 [https://doi.org/10.1016/S1995-7645\(11\)60149-1](https://doi.org/10.1016/S1995-7645(11)60149-1)
- Neilan Rachael Miller, Schaefer Elsa, Gaff Holly, Fister Katherine, Lenhart Suzanne (2010) Modeling optimal intervention strategies for cholera. *Bulletin of Mathematical Biology* 72:2004–18. <https://doi.org/10.1007/s11538-010-9521-8>
- Mukandavire Z, Tripathi A, Chiyaka C, Musuka G, Nyabadza F, Mwambi HG (2011) Modelling and analysis of the intrinsic dynamics of cholera. *Differential Equations and Dynamical Systems* 19:253–265

- Murphy Kenneth M, Travers Paul, Walport Mark (2007) *Janeway's Immunobiology*. Garland Science, 7th edition
- John Mwaba, Amanda K Debes, Patrick Shea, Victor Mukonka, Orbric Chew, Caroline Chisenga, Michelo Simuyandi, Geoffrey Kwenda, David Sack, Roma Chilengi, et al. Identification of cholera hotspots in zambia: A spatiotemporal analysis of cholera data from 2008 to 2017. *PLoS neglected tropical diseases*, 14(4):e0008227, 2020
- Nelson Eric J, Harris Jason B, Morris Jr J Glenn, Calderwood Stephen B, Camilli Andrew (2009) Cholera transmission: the host, pathogen and bacteriophage dynamic. *Nature Reviews Microbiology*, 7(10):693–702
- Ngwa MC, Young A, Liang S, Blackburn J, Mouhaman A, Morris JG, Jr. Cultural influences behind cholera transmission in the Far North Region, Republic of Cameroon: a field experience and implications for operational level planning of interventions. *The Pan African medical journal*, 28:311, 2017. <https://doi.org/10.11604/pamj.2017.28.311.13860>
- Ng' Ombe Harriet, Simuyandi Michelo, Mwaba John, et al. (2022) Immunogenicity and waning immunity from the oral cholera vaccine (shanchol™) in adults residing in lukanga swamps of zambia. *Plos one*, 17(1):e0262239,
- Orimbo Erick Otieno, Oyugi Elvis, Dulacha Diba, Obonyo Mark, Hussein Abubakar, Githuku Jane, Owiny Maurice, Gura Zeinab (2020) Knowledge, attitude and practices on cholera in an arid county, kenya, 2018: A mixed-methods approach. *PLoS one*, 15(2):e0229437,
- Pan American Health Organization. Cholera outbreak in Hispaniola 2023 - Situation Report 15. Retrieved May 16, 2024, from <https://www.paho.org/en/documents/cholera-outbreak-hispaniola-2023-situation-report-15>
- Rinaldo A, Bertuzzo E, Mari L, Righetto L, Blokesch M, Gatto M, Casagrandi R, Murray M, Vesenbeckh SM, Rodriguez-Iturbe I (2012) Reassessment of the 2010–2011 haiti cholera outbreak and rainfall-driven multiseason projections. *Proceedings of the National Academy of Sciences of the United States of America* 109(17):6602–6607. <https://doi.org/10.1073/pnas.1203333109>
- Root Elisabeth Dowling, Rodd Joshua, Yunus Mohammad, Emch Michael (2013) The role of socioeconomic status in longitudinal trends of cholera in matlab, bangladesh, 1993–2007. *PLoS neglected tropical diseases*, 7(1):e199
- Sinyange Nyambe, Cholera epidemic-lusaka, zambia, (2018) MMWR. Morbidity and Mortality Weekly Report 67:2018 october 2017-may
- Tappero Jordan, Tauxe Robert (2011) Lessons Learned during Public Health Response to Cholera Epidemic in Haiti and the Dominican Republic. *Emerging Infectious Diseases* 17(11). <https://doi.org/10.3201/eid1711.110827>
- Taylor Dawn L, Kahawita Tanya M, Cairncross Sandy, Ensink Jeroen HJ (2015) The impact of water, sanitation and hygiene interventions to control cholera: a systematic review. *PLoS one*, 10(8):e0135676
- Jin Wang (2022) Mathematical models for cholera dynamics-a review. *Microorganisms* 10(12):2358
- Wang Xueying, Wang Jin (2015) Analysis of cholera epidemics with bacterial growth and spatial movement. *Journal of Biological Dynamics* 9(sup1):233–261
- World Health Organization. Cholera. <https://www.who.int/news-room/fact-sheets/detail/cholera>, 2023. Accessed: 2024-08-27
- World Health Organization Data. Life expectancy at birth (years). Retrieved July 22, 2024, from <https://data.who.int/indicators/i/A21CFC2/90E2E48>
- Yang Chayu, Wang Jin (2019) A cholera transmission model incorporating the impact of medical resources. *Mathematical Biosciences and Engineering* 16(5):5226–5246
- Zuckerman Jane N, Rombo Lars, Fisch Alain (2007) The true burden and risk of cholera: implications for prevention and control. *The Lancet infectious diseases* 7(8):521–530

**Publisher's Note** Springer Nature remains neutral with regard to jurisdictional claims in published maps and institutional affiliations.

Springer Nature or its licensor (e.g. a society or other partner) holds exclusive rights to this article under a publishing agreement with the author(s) or other rightsholder(s); author self-archiving of the accepted manuscript version of this article is solely governed by the terms of such publishing agreement and applicable law.